Small-Angle X-ray Scattering Study of Au Nanoparticles Dispersed in the Ionic Liquids 1-Alkyl-3-methylimidazolium Tetrafluoroborate

ARTICLE *in* THE JOURNAL OF PHYSICAL CHEMISTRY C · MARCH 2009

Impact Factor: 4.77 · DOI: 10.1021/jp807046u

5 AUTHORS, INCLUDING:

Yoshikiyo Hatakeyama
Chiba University
28 PUBLICATIONS **174** CITATIONS
SEE PROFILE

Keiko Nishikawa
Chiba University
217 PUBLICATIONS **3,964** CITATIONS
SEE PROFILE

Article

Small-Angle X-ray Scattering Study of Au Nanoparticles Dispersed in the Ionic Liquids 1-Alkyl-3-methylimidazolium Tetrafluoroborate

Yoshikiyo Hatakeyama, Maimi Okamoto, Tsukasa Torimoto, Susumu Kuwabata, and Keiko Nishikawa

J. Phys. Chem. C, **2009**, 113 (10), 3917-3922• DOI: 10.1021/jp807046u • Publication Date (Web): 13 February 2009

Small-Angle X-ray Scattering Study of Au Nanoparticles Dispersed in the Ionic Liquids 1-Alkyl-3-methylimidazolium Tetrafluoroborate

Yoshikiyo Hatakeyama,[†] Maimi Okamoto,[‡] Tsukasa Torimoto,[§] Susumu Kuwabata,[||] and Keiko Nishikawa*[,‡]

Graduate School of Science and Technology, and Graduate School of Advanced Integration Science, Chiba University, Chiba 263-8522, Japan, Graduate School of Engineering, Nagoya University, Nagoya 464-8603, Japan, and Graduate School of Engineering, Osaka University, Suita, Osaka 565-0871, Japan

Received: August 7, 2008; Revised Manuscript Received: December 23, 2008

It was recently discovered that the sputter deposition of metal onto the surface of an ionic liquid generates nanoparticles in the liquid with no additional stabilizing agents. We performed small-angle X-ray scattering (SAXS) experiments to investigate the structure of Au nanoparticles synthesized by this method and to reveal the properties of the ionic liquid that affect the formation process. For a systematic study of these properties, we selected imidazolium-based ionic liquids with different alkyl chain lengths fixing the anion BF_4^-. The Au concentration dependence for the formation of the nanoparticles was also studied. The SAXS results revealed that Au nanoparticles with 0.75−3.5 nm diameter were generated under the experimental conditions and that the particle size was relatively uniform for a fixed condition. The results demonstrated that the particle size depends on the type of ionic liquid and on the concentration if the ionic liquid is fixed. Integrating the experimental results, it was concluded that the surface tension and viscosity of the ionic liquid played important roles in conjunction with the Au concentration. It was interpreted that the surface tension influences the initial formation process of nanoparticles on the surface of an ionic liquid, and the viscosity affects the aggregation process during the dispersion of the Au particles from the surface into the liquid.

1. Introduction

Room temperature ionic liquids are attractive materials that are expected to fit into several fields of application[1−5] because they have many unique physicochemical properties, such as low melting points despite their ionic characters, high thermal stabilities, high ionic conductivities, and the ability to dissolve different types of substances. Moreover, owing to their extremely low vapor pressures,[6] ionic liquids can be treated under high vacuum conditions and are regarded as fruitful media for vacuum sciences and technologies. X-ray photoelectron spectroscopy[7] and scanning electron microscope[8] experiments are the pioneering examples. Torimoto et al. recently reported an extremely clean and simple method using a sputter deposition technique to synthesize Au nanoparticles in ionic liquids.[9] It is a novel method, since metal nanoparticles can be synthesized without any additional stabilizing agents. This method is applicable for synthesizing not only other single-metal nanoparticles but also alloy nanoparticles.[10]

In recent years, metal nanoparticles in ionic liquids have been actively studied[11] because the ionic liquids containing metal nanoparticles are regarded as good reaction fields for the following reasons: first, ionic liquids are the media whose functions can be designed, and second, most metal nanoparticles exhibit characteristic catalytic activities. Like nanoparticles dispersed in liquids, metal nanoparticles also exhibit unique photonic and electrical properties that are interesting for extensive applications such as biosensors, catalysts, optics, and electronics.[12−16] In most cases, these useful properties and functions are affected by the size and size distribution of particles. Therefore, the techniques of synthesizing the nanoparticles with the desired size and careful structural characterization are required for further applications.

In the previous study on the novel method to synthesize Au nanoparticles in ionic liquids, some of us (T.T. and S.K.) reported rough estimations of the size and the Au-concentration dependences from the surface plasmon resonance peak of Au nanoparticles.[9] In the present study, we performed detailed small-angle scattering experiments to analyze the size and size distribution of Au nanoparticles dispersed in several ionic liquids. The present results led us to the factors that determine the size of the Au nanoparticles.

2. Experimental Section

2.1. Samples. To elucidate the effect of the alkyl chain length on the formation of Au nanoparticles, we selected three types of imidazolium-based ionic liquids fixing the anion BF_4^-, namely, 1-ethyl-3-methylimidazolium tetrafluoroborate (C_2mim^+/BF_4^-), 1-buthyl-3-methylimidazolium tetrafluoroborate (C_4mim^+/BF_4^-), and 1-methyl-3-octylimidazolium tetrafluoroborate (C_8mim^+/BF_4^-). Ionic liquids C_2mim^+/BF_4^- and C_4mim^+/BF_4^- were purchased from Kanto Chemical. They were almost colorless, and their purities were guaranteed to be better than 95%. C_8mim^+/BF_4^- from Wako Pure Chemical Industries was light yellow, and its purity was guaranteed to be better than 98%.

For most ionic liquids, it is commonly known that adventitious water immensely affects their physical and chemical properties. So, all the samples were dried for 24 h at 333 K under a vacuum of about 10^{-3} Pa and kept under an argon

* Corresponding author: E-mail: k.nishikawa@faculty.chiba-u.jp.
[†] Graduate School of Science and Technology, Chiba University.
[‡] Graduate School of Advanced Integration Science, Chiba University.
[§] Nagoya University.
[||] Osaka University.

10.1021/jp807046u CCC: $40.75
Published on Web 02/13/2009

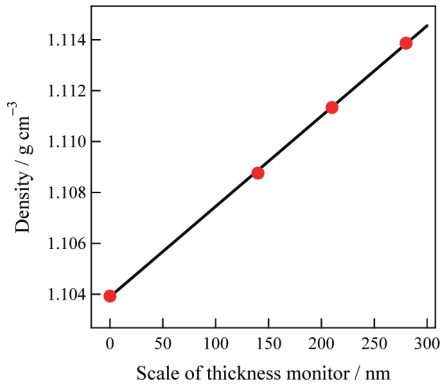

Figure 1. Relationship between the scales of the thickness monitor and the densities of Au-dispersed C_8mim^+/BF_4^-.

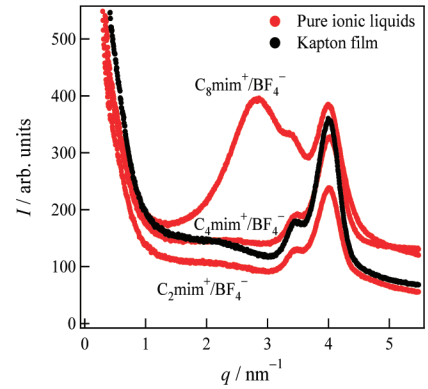

Figure 2. SAXS profiles of the pure ionic liquids C_2mim^+/BF_4^-, C_4mim^+/BF_4^-, and C_8mim^+/BF_4^- (red curves) and that of the empty sample holder with Kapton windows (black curve).

atmosphere before the sputter deposition. The amount of water was estimated by Karl Fischer's method and was less than 20 ppm.

2.2. Sputter Deposition of Au. Au nanoparticles were prepared by sputter deposition onto ionic liquids.[9] Using a sputter coater (JFC-1500, JEOL), the deposition was performed at a voltage of 1 kV and a current of 5 mA under argon pressure of 10−15 Pa at room temperature. Each ionic liquid (1 cm^3) was spread on a Teflon plate (6.1 cm^2) that was horizontally set in the sputter coater. The liquid surface was located at a distance of 25 mm from the gold foil target (99.99% in purity). The sputtering times were 12−36 min. During the sputter deposition, all ionic liquids turned dark red due to the dispersion of Au particles into the liquids.

The film thickness monitor of the sputter coater was used as a guide for the amount of the deposited Au. After the sputter deposition, densities of Au-dispersed ionic liquids were measured by a vibrating-tube densitometer (DMA4500, Anton Paar) at 295.15 K under atmospheric pressure. Figure 1 shows the relationship between the values of the thickness monitor and the densities of Au-dispersed C_8mim^+/BF_4^-. The linear relationship shows that the thickness monitor can be used as a scale for the amount of dispersed Au. Approximate concentrations of Au were estimated using the density of bulk gold for simplicity. The values of the thickness monitor for this experimental condition, 140, 210, and 280 nm, correspond to 27, 40, and 53 mmol/dm^3, respectively. In the present experiment, the concentrations of Au in the ionic liquids were fixed to these values.

2.3. SAXS Measurements. Small-angle scattering intensities were measured using a laboratory-scale SAXS apparatus (NANO-Viewer, RIGAKU). Using a multilayer mirror, X-rays, emitted from a rotating Cu target of an X-ray generator, were monochromatized to $\lambda = 0.154$ nm (λ, the wavelength of the X-ray) and were focused to the beam with a diameter of 0.4 mm at the sample position. The camera length was set to 400 mm. All X-ray paths except the sample position were maintained in vacuum of about 10^{-1} Pa in order to avoid the X-ray scattering from air. The SAXS intensity was measured using a two-dimensional detector (imaging plate), and the positional resolution of the imaging plate was 50 μm. The observable q-region in the measurements was 0.24−5.5 nm^{-1}, where the scattering parameter q is defined as $q = (4\pi \sin \theta)/\lambda$ (2θ, the scattering angle of X-rays). The intensity of incident X-rays was monitored using a micro-ionization chamber (REPIC). In order to experimentally determine the absorption factor of a sample, the intensities of transmitted X-rays of the Au-dispersed ionic liquid and the pure one were measured every time before the SAXS intensity measurements by an ionization chamber (OKEN), which was set instead of the imaging plate.

For SAXS measurements, each ionic liquid was packed in a sample holder with windows of polyimide (Kapton) thin films. The inner size of the sample holder was 6 mm in diameter and 0.3 mm in thickness. The thickness was adjusted by a Teflon spacer. Because of the hygroscopic property of ionic liquids, all operations for sampling were performed under an argon atmosphere. The accumulation time for measurement of scattering intensity from a sample was 1800 s. The obtained data were corrected for the intensity fluctuation of incident X-rays, background intensity, and the effect of absorption. In data correction, the scattering intensity of the corresponding pure ionic liquid was used as the background intensity; i.e., the intensity of scattering from the Au nanoparticles, I_{Au}, is obtained by

$$I_{Au} = I_{obs} \exp(\mu_{Au} l) - I_{IL} \quad (1)$$

where I_{obs} and I_{IL} are the observed scattering intensities of the Au-dispersed ionic liquid and the corresponding pure one, respectively, μ_{Au} is the linear absorption coefficient of Au in the ionic liquid, and l is the sample thickness. The absorption factor $\mu_{Au}l$ was determined experimentally by measurements of transmitted intensities of the Au-dispersed ionic liquid and the pure one.

3. Results and Discussion

3.1. SAXS Profiles. In Figure 2, the SAXS profiles of the three neat ionic liquids (red curves) are shown together with the profile of the empty sample holder (a black curve). These curves represent the raw scattering intensities. Note that most scattering intensity in the smaller q-region and the peak at $q = 4$ nm^{-1} are from the Kapton films of windows of the sample holder, and the peak at $q = 3.5$ nm^{-1} is assigned to the scattering from the Kapton window of the vacuum chamber. Only C_8mim^+/BF_4^- has a characteristic peak at $q = 2.8$ nm^{-1}, which is due to the structural correlation formed by the long alkyl chains. Triolo et al. also observed similar peaks in the scattering profiles of ionic liquids with long alkyl chains.[17,18] For comparison of the raw scattering intensities from Au-dispersed ionic liquids (blue curves) and the raw neat ionic liquid (a black curve), the series of C_4mim^+/BF_4^- are shown in Figure 3 as an example. Note that the scattering intensities in the smaller q-region, which contains the main information on the structure of Au nanoparticles, are 10−20 times stronger than the intensity of the neat ionic liquid. The

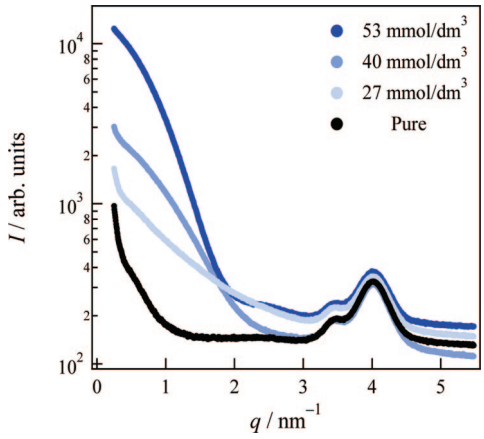

Figure 3. Comparison of the raw scattering intensities from Au-dispersed C_4mim^+/BF_4^- (blue curves) and the raw neat ionic liquid (a black curve).

successful removal of these parasitic scatterings depends on the precision of the absorption factors mentioned in section 2.3. We consider that the determination of the factor was performed with sufficient precision because the determination was made at each measurement of SAXS intensities. Using a standard sample such as water, we examined the effectiveness of our correction procedures for the subtraction of parasitic scattering intensities and obtained satisfactory results.

Parts a, b, and c of Figure 4 display the scattering profiles of Au nanoparticles dispersed in C_2mim^+/BF_4^-, C_4mim^+/BF_4^-, and C_8mim^+/BF_4^-, respectively, after the corrections for the intensity fluctuation of incident X-rays, the background intensities, and the absorption effects. Three curves in each figure refer to I_{Au} for the 27, 40, and 53 mmol/dm^3 Au solutions. First, it is observed that scattering intensities increase in the lower q-region as Au concentration increases. This shows that concentration dependences exist for the formation of Au nanoparticles.

The second major characteristic of the SAXS profiles is the appearance of the shoulders at $q = 2.8-3.0$ nm^{-1}. The appearances have three origins: (i) the SAXS profile of Au nanoparticles, (ii) the residual errors in the background correction of the corresponding pure ionic liquid, and (iii) the structural correlation between Au nanoparticles. For the C_2mim^+/BF_4^- and C_4mim^+/BF_4^- series, origin ii can be excluded because the scattering profiles of the neat ionic liquids have no hump in this region, as shown in Figure 2. However, we cannot completely exclude the possibility of origin ii for the C_8mim^+/BF_4^- series. The strong parasitic scattering from the Kapton films of the windows may be removed completely by our correction procedure. This suggests that the contribution from the scattering peak of C_8mim^+/BF_4^- seems to be successfully removed. To examine the possibility of origin iii, we performed the SAXS measurement for a sample that was diluted to about half the concentration of the 53 mmol/dm^3 solution of C_2mim^+/BF_4^-. As shown in Figure 5, the scattering intensity of the diluted solution proportionally decreased from that of the original sample, without any change in the profile. This result proves that Au nanoparticles exist independently without structural correlation even for the thickest solution. Thus, it is confirmed that there is no possibility of origin iii.

Therefore, we can conclude that the humps at $q = 2.8-3.0$ nm^{-1} are due to origin i and are assigned to the second maximum peaks of the scattering intensity from the nanoparticles. For a spherical particle with homogeneous electron density, its X-ray scattering intensity is expressed by the following equation:

$$I_{sphere} = A\{\sin(qR) - (qR)\cos(qR)\}^2/q^6 \qquad (2)$$

where R is the radius of the sphere and A is a constant value depending on the number density of the particles, the scattering factor of the constituent atoms, and the experimental conditions. The appearances of the second peaks for most samples show that Au nanoparticles in each solution have almost similar sizes. When many spheres with slightly different radii are dispersed, the peaks and the valley of the scattering curves are blurred. As for 53 mmol/dm^3 solution of C_2mim^+/BF_4^-, the dispersion for the averaged radius is simulated to be approximately 20%. We will discuss in detail the distribution of the particle size in section 3.2.

3.2. Simulation of SAXS Profiles. It is well-known that the Guinier analysis[19] is the most popular and simple method in the treatment of SAXS data. However, we presented the results of simulation study using the overall experimental profiles, because the Guinier regions of the present samples were very narrow for the measurable q region of our apparatus and we obtained the SAXS profiles of wider regions than the Guinier ones, including the swell of the scattering intensities of the nanoparticles. The size-distribution of the scatterers should be considered in the simulation, since dispersion in size around the average value is suggested by the smearing of the first minimum, as shown in Figure 4a−c. The curve fitting by theoretical scattering curves was performed, assuming that the nanoparticles are spherical and

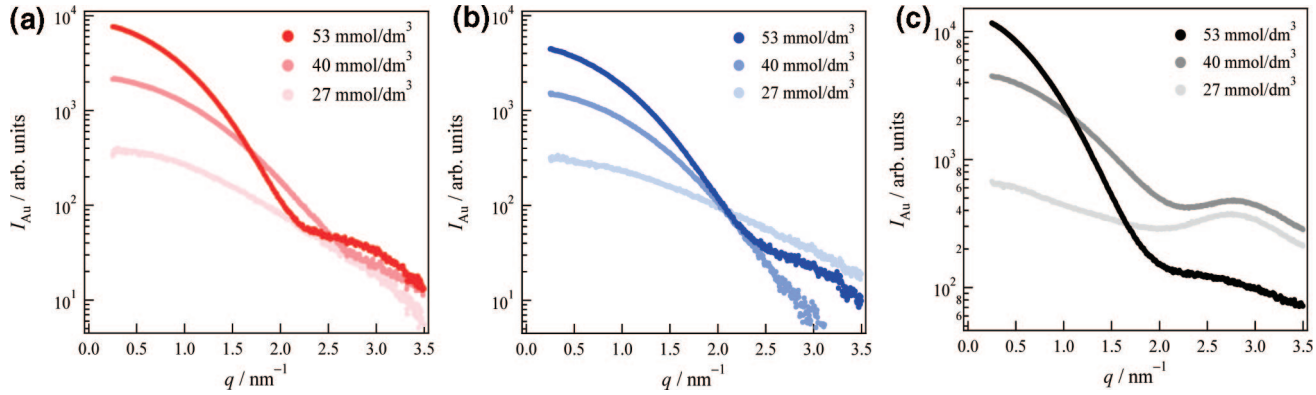

Figure 4. Scattering profiles of Au nanoparticles dispersed in (a) C_2mim^+/BF_4^-, (b) C_4mim^+/BF_4^-, and (c) C_8mim^+/BF_4^-.

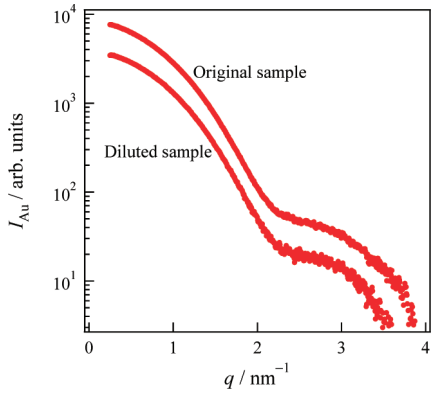

Figure 5. Comparison between the SAXS profile of the 53 mmol/dm^3 solution of C_2mim^+/BF_4^- and that of the sample diluted to approximately half-concentration.

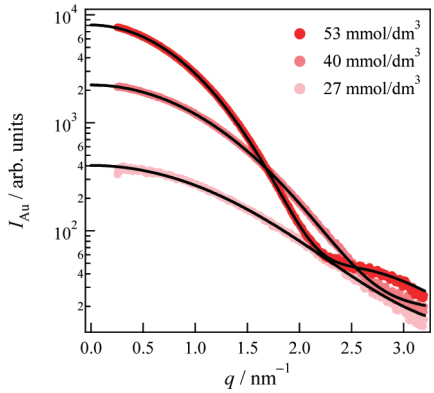

Figure 6. Profile fittings of SAXS intensities for the C_2mim^+/BF_4^- series. Red and pink curves are experimental curves, and black curves are simulated ones via the Γ distribution.

that the size distribution is expressed by the Γ distribution described by

$$P_{R_0}^{M}(R) = \frac{1}{\Gamma(M)}\left(\frac{M}{R_0}\right)^{M} \exp\left(-\frac{MR}{R_0}\right) R^{-1+M} \qquad (3)$$

In eq 3, Γ is the gamma function, R_0 is average radius, and M is a parameter for the distribution of the particle size and is related to the dispersion σ as given by

$$\sigma(\%) = \frac{\sqrt{\langle \delta R^2 \rangle}}{R_0} \times 100 = \frac{1}{\sqrt{M}} \times 100 \qquad (4)$$

The scattering intensity for a spherical scatterer with the radius R is given by eq 2.

Figure 6 displays experimental scattering data (red and pink dots) and theoretical scattering curves (black curves) for the C_2mim^+/BF_4^- series. As shown in the figure, the theoretical curves simulate the experimental intensities very well. Although not displayed here, the excellent agreements were also obtained between experimental intensities and theoretical curves for the C_4mim^+/BF_4^- and C_8mim^+/BF_4^- series as well. The particle size distributions for the series of the three ionic liquids are shown in Figure 7. The curves indicate the distributions referring to the number of particles[20] vs the diameter, and they are normalized by the area to highlight the widths of dispersion. In Figure 8, the values of the diameter at the peak-top are plotted against concentration. Their values indicate the diameters of the most abundant particles.

From Figures 7 and 8, we summarize the key points of the formation of Au nanoparticles in the three ionic liquids as follows.

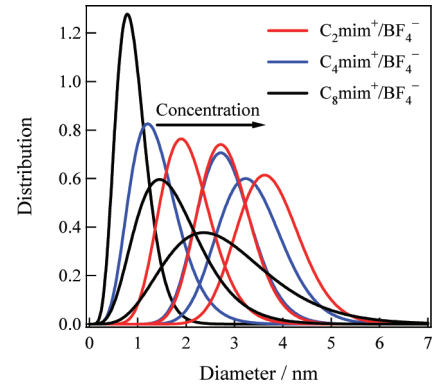

Figure 7. Particle size distributions for the C_2mim^+/BF_4^- (red curves), C_4mim^+/BF_4^- (blue curves), and C_8mim^+/BF_4^- series (black curves). As the concentration increases, the size of the Au particles increases.

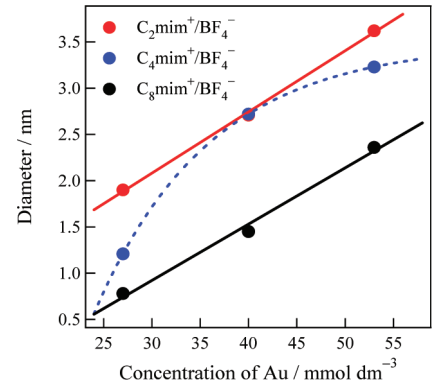

Figure 8. Diameters of the most abundant particles vs. Au concentration. Red, blue, and black points correspond to the C_2mim^+/BF_4^-, C_4mim^+/BF_4^-, and C_8mim^+/BF_4^- series, respectively.

TABLE 1: Viscosity and Surface Tension of Ionic Liquids

ionic liquid	surface tension/mN m^{-1}	viscosity/cP (293 K)
C_2mim^+/BF_4^-	54.4 (at 298.15 K)[22]	66.5[24]
C_4mim^+/BF_4^-	44.81 (at 293.15 K)[23]	154[24]
C_8mim^+/BF_4^-	33.62 (at 293.15 K)[23]	439[24]

(1) The sizes of Au nanoparticles generated by sputtering deposition are relatively uniform and are 0.75−2.0 nm in diameter with the dispersion of 20−30% for the lower concentration such as 27 mmol/dm^3.

(2) These sizes increase as the Au concentration increases.

(3) The particle size is dependent on the ionic liquids.

(4) The dispersion of the sizes increases as the Au concentration increases for an ionic liquid. Comparing the three series, the dispersion of C_8mim^+/BF_4^- changes drastically as the concentration rises.

As for the particle size and their distributions, details are discussed in the next section.

3.3. Dependence of Ionic Liquids on Formation of Au Nanoparticles. It is well-known that the Ar^+ bombardment of Au causes the physical ejection of Au atoms and/or small clusters.[21] As shown in Figures 7 and 8, nanoparticles increase their diameter as a function of concentration, and their sizes are dependent on the ionic liquids. These facts show that the growth of nanoparticles occurs by the aggregation of sputtered Au atoms and/or clusters after touching these liquids. We believe that the final concentration after dispersion of Au into the ionic liquid, however, is not the ultimate factor to determine the particle size. The reason is that the samples of several batches with the same concentration under different sputtering conditions

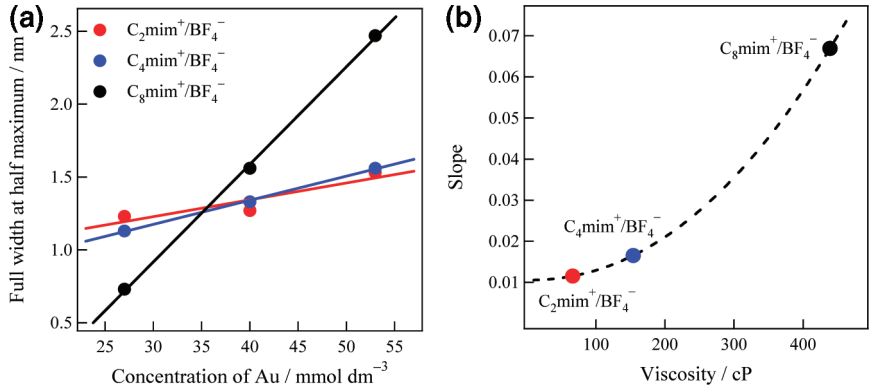

Figure 9. (a) Full width at half-maximum of particle size distribution vs Au concentration. Red, blue, and black points correspond to the C_2mim^+/BF_4^-, C_4mim^+/BF_4^-, and C_8mim^+/BF_4^- series, respectively. (b) The slope of the line in part a vs the viscosity of the corresponding pure ionic liquid.

showed different results. This supposition is also derived from the fact that the SAXS profile after dilution is similar to that of the original solution (Figure 5). As a result, it is interpreted that the aggregation of Au atoms and/or clusters occurs on the surface of the ionic liquid and beginnings of the Au dispersion into the ionic liquid.

The Au atoms and/or clusters generated by the Ar^+ bombardment first deposit on the surface of the ionic liquid. Therefore, it is considered that the surface tension of the ionic liquid has a significant role on the formation of Au nanoparticles. Considering that the following process is a dispersion of Au particles into the ionic liquid, the viscosity of the ionic liquid also plays an important role. Table 1 shows the values of surface tension and viscosity for the ionic liquids of the present study.

Let us now consider the effect of surface tension of ionic liquids. The surface tensions of the ionic liquids decrease as the alkyl chain length increases.[23,25] The results from theoretical curve fittings indicate that the larger surface tension causes the formation of larger particles. We believe that this tendency is induced by the difference of the staying time of Au clusters on the surface of the ionic liquid. The Au atoms and/or clusters remain longer on the surface of the ionic liquids with higher surface tensions. The experimental results support the supposition that the aggregation of Au clusters first occurs on the surface of an ionic liquid; i.e., the surface tension is important for the formation of nanoparticles at lower concentrations.

After the deposition on the surface of the ionic liquid, Au nanoparticles start to disperse into the liquid. At that time, the diffusion velocity related to the viscosity of the ionic liquid influences the aggregation processes of the nanoparticles. For C_8mim^+/BF_4^-, we believe that the nanoparticles cannot disperse faster due to the higher viscosity and that the larger concentration area is formed in the vicinity of the surface. The large particles seem to be formed in this larger concentration area.

In Figure 9a, the full widths at half-maximum for the distribution curves (Figure 7) are plotted against the Au concentration, and a good linear relationship exists between them. The width enlargement due to the increase in the Au concentration seems to be reflected by the aggregation process of the higher concentration area formed in the vicinity of the surface. Figure 9b shows the plots of the slopes for the lines in Figure 9a against the viscosity. This relationship suggests that the ionic liquid with larger viscosity promotes the aggregation processes, thereby generating nanoparticles of various sizes. It is concluded that the ionic liquid with lower surface tension and lower viscosity is suitable to generate smaller and more uniform Au nanoparticles.

We discuss so far the factors influencing the size of Au nanoparticles, focusing on the aggregation process of clusters. Since ionic liquids themselves work as stabilizers, they should also determine the size and size distribution. It is commonly known that the surface of a metal nanoparticle is electron-deficient. It has been pointed out that, even for chemically synthesized metal nanoparticles, their stabilization in ionic liquids is due to the positive charge on the surface of the particles.[26,27] In the present study, the surface-adsorbed anion of the ionic liquids is fixed as BF_4^-. The second coordination shell seems to be formed by cations of C_2mim^+, C_4mim^+, and C_8mim^+. Although the length of alkyl chains affects the stability of the Au nanoparticle, its effect is not as strong as that by anions. Therefore, we are currently investigating the anion effects on the Au nanoparticles in ionic liquids.

4. Conclusion

By SAXS measurements, we studied structures of Au nanoparticles prepared in three imidazolium-based ionic liquids by the sputter deposition technique. We focused on the alkyl chain length dependence for the formation of Au nanoparticles, fixing the anion in BF_4^-. The SAXS intensities were analyzed by the profile fitting of theoretical scattering curves. Comparison of the results showed that the surface tensions and viscosities of ionic liquids are important for synthesis by sputter deposition. In particular, surface tension has a significant role on the characteristics of nanoparticles; i.e., the first step of aggregation of Au atoms and/or small clusters occurs mainly on the surface of an ionic liquid forming smaller nanoclusters. The viscosity of an ionic liquid affects the dispersion of the nanoparticles. Especially, the aggregation of Au nanoparticles in high concentration area for higher viscosity ionic liquids is the second step and causes a wider distribution in the size of nanoparticles. As a result of this study, we can control the size and dispersion of Au nanoparticles by the regulation of the concentration of the ejected Au atoms and/or smaller clusters on the surface of an ionic liquid and in the vicinity of the surface.

Acknowledgment. This study has been supported by a Grand-in-Aid for Scientific Research (No. 17073002 for K.N. and No. 17073014 for S.K.) on Priority Area "Science on Ionic Liquids" (Area number: 452) from the Ministry of Education, Culture, Sports, Science and Technology of Japan.

References and Notes

(1) Greaves, T. L.; Drummond, C. J. *Chem. Rev.* **2008**, *108*, 206–237.
(2) Plechkova, N. V.; Seddon, K. R. *Chem. Soc. Rev.* **2008**, *37*, 123–150.
(3) Wei, D.; Ivaska, A. *Anal. Chim. Acta* **2008**, *607*, 126–135.
(4) Angell, C. A.; Byrne, N.; Belieres, J. *Acc. Chem. Res.* **2007**, *40*, 1228–1236.

(5) Han, X.; Armstrong, D. W. *Acc. Chem. Res.* **2007**, *40*, 1079–1086.

(6) Earle, M. J.; Esperanca, J. M. S. S.; Gilea, M. A.; Canongia Lopes, J. N.; Rebelo, L. P. N.; Magee, J. W.; Seddon, K. R.; Widegren, J. A. *Nature* **2006**, *439*, 831–834.

(7) Smith, E. F.; Garcia, I. J. V.; Briggs, D.; Licence, P. *Chem. Commun.* **2005**, 5633–5635.

(8) Kuwabata, S.; Kongkanand, A.; Oyamatsu, D.; Torimoto, T. *Chem. Lett.* **2006**, *35*, 600–601.

(9) Torimoto, T.; Okazaki, K.; Kiyama, T.; Hirahara, K.; Tanaka, N.; Kuwabata, S. *Appl. Phys. Lett.* **2006**, *89*, 243117.

(10) Okazaki, K.; Kiyama, T.; Hirahara, K.; Tanaka, N.; Kuwabata, S.; Torimoto, T. *Chem. Commun.* **2008**, 691–693.

(11) Migowski, P.; Dupont, J. *Chem. Eur. J.* **2007**, *13*, 32–39.

(12) Schmid, G. *Chem. Rev.* **1992**, *92*, 1709–1727.

(13) Templeton, A. C.; Wuelfing, W. P.; Murray, R. W. *Acc. Chem. Res.* **2000**, *33*, 27–36.

(14) Jana, N. R.; Gearheart, L.; Murphy, C. J. *Chem. Mater.* **2001**, *13*, 2313–2322.

(15) Burda, C.; Chen, X.; Narayanan, R.; El-Sayed, M. A. *Chem. Rev.* **2005**, *105*, 1025–1102.

(16) Sawai, Y.; Takimoto, B.; Nabika, H.; Ajito, K.; Murakoshi, K. *Faraday Discuss.* **2006**, *132*, 179–190.

(17) Triolo, A.; Russina, O.; Fazio, B.; Triolo, R.; Di Cola, E. *Chem. Phys. Lett.* **2008**, *457*, 362–365.

(18) Triolo, A.; Russina, O.; Bleif, H.-J.; Di Cola, E. *J. Phys. Chem. B* **2007**, *111*, 4641–4644.

(19) Guinier, A.; Fournet, G. *Small-Angle Scattering of X-rays*; Academic Press, London, 1955.

(20) Lindner, P.; Zemb, Th., Eds. *Neutrons, X-rays, and Light: Scattering Methods Applied to Soft Condensed Matter*; Elsevier: Amsterdam, 2002.

(21) Behrisch, R.; Wittmaack, K., Eds. *Sputtering by Particle Bombardment III*; Springer: Berlin, 1991.

(22) Zhou, Z.; Matsumoto, H.; Tatsumi, K. *ChemPhysChem.* **2005**, *6*, 1324–1332.

(23) Freire, M. G.; Carvalho, P. J.; Fernandes, A. M.; Marrucho, I. M.; Queimada, A. J.; Coutinho, J. A. P. *J. Colloid Interface Sci.* **2007**, *314*, 621–630.

(24) Seddon, K.; Stark, A.; Torres, M. *ACS Symp. Ser.* **2002**, *819*, 34–49.

(25) Ghatee, M. H.; Zolghadr, A. R. *Fluid Phase Equilib.* **2008**, *263*, 168–175.

(26) Özkar, S.; Finke, R. G. *J. Am. Chem. Soc.* **2002**, *124*, 5796–5810.

(27) Scheeren, C. W.; Machado, G.; Teixeira, S. R.; Morais, J.; Domingos, J. B.; Dupont, J. *J. Phys. Chem. B* **2006**, *110*, 13011–132020.

JP807046U